On an efficient numerical method for modeling sea ice dynamics

Jinlun Zhang

Polar Science Center, University of Washington, Seattle

W. D. Hibler III

Thayer School of Engineering, Dartmouth College, Hanover, New Hampshire

Abstract. A computationally efficient numerical method for the solution of nonlinear sea ice dynamics models employing viscous-plastic rheologies is presented. The method is based on a semi-implicit decoupling of the x and y ice momentum equations into a form having better convergence properties than the coupled equations. While this decoupled form also speeds up solutions employing point relaxation methods, a line successive overrelaxation technique combined with a tridiagonal matrix solver procedure was found to converge particularly rapidly. The procedure is also applicable to the ice dynamics equations in orthogonal curvilinear coordinates which are given in explicit form for the special case of spherical coordinates.

1. Introduction

A prominent feature of sea ice in the polar regions is its almost ceaseless motion. In sea ice dynamics models, ice motion is typically described by momentum equations that treat the ice cover as a two-dimensional continuum. It has also long been recognized that ice interaction is a complicated physical process having a highly nonlinear nature. In recent years a number of nonlinear plastic ice rheologies have been used [*Coon et al.*, 1974; *Pritchard et al.*, 1977; *Hibler*, 1979; *Flato and Hibler*, 1992; *Ip et al.*, 1991] for modeling this nonlinear ice interaction in the sea ice momentum equations. The viscous-plastic method proposed by *Hibler* [1979] for modeling plastic flow has found wide utility since it provides a means to model a variety of relatively realistic yet complex plastic constitutive laws of high nonlinearity. The essential idea in the "viscous-plastic" method [*Hibler*, 1979] is to approximate the rigid or elastic portion of a plastic continuum by a state of very slow creep.

The introduction of nonlinear ice interaction forces into the momentum equations substantially increases the difficulty of solution [e.g., *Hibler*, 1979]. The main reason for this is that the inclusion of a plastic rheology with resistance to compression prevents the two momentum equations for u and v velocity components from being combined into one complex velocity equation as is typically done in boundary layer models [e.g., *McPhee*, 1986; *Thorndike and Colony*, 1982]. Of course, coupled equations like those of *Hibler* [1979] can be solved using explicit time-stepping methods which are almost fully optimizable on vector computers or multiprocessors [e.g., *Ip et al.*, 1991]. However, the time step must be very small to obtain stable solutions, so that the advantage of full optimization is more than offset by the very small time step. As a consequence, explicit methods are not practical except for very limited applications.

A computationally efficient semi-implicit method was pro-

posed by *Hibler* [1979] to solve the momentum equations including a plastic rheology with an elliptical yield curve. This method is a combination of a modified Euler time step scheme and a point successive relaxation procedure. At each time step the modified Euler time-marching procedure is used to center the nonlinear terms and to advance to the next time step. This requires a computationally intensive point relaxation to be conducted twice in each time step to solve the linearized implicit coupled equations for ice velocity components u and v. Due to the linearization of the bulk and shear viscosities in the semi-implicit method, the solution at each time step yields only an approximation to plastic flow. However, by repeating the semi-implicit procedure a number of times at each physical time step, a true plastic solution may be obtained. This basic semi-implicit procedure has recently been extended by *Ip* [1993] to include a variety of more complex plastic yield curves.

While functional at low resolution, this point successive relaxation method is not computationally efficient for large grids of high resolution. One of the reasons for the inefficiency is that either relaxation or limited overrelaxation must be used because of the complexity of the coupled u and v equations [*Ames*, 1977]. In addition, it has been found that with point relaxation, the rate of convergence depends strongly on the maximum viscosity or "creep" parameter existing in the grid. Lowering this value can speed convergence but also results in a less realistic solution of plastic flow.

Recently, *Oberhuber* [1990] [see also *Holland et al.*, 1993] used a variation on line successive overrelaxation to solve the viscous-plastic ice momentum equations modified to a spherical coordinate system. In his method a variation on row relaxation is used in row-by-row sweeping in the model's finite difference grid, with ice velocity u and v at each row solved directly and simultaneously using an efficient tridiagonal matrix solver. However, while an improvement on the point relaxation method, this method still focuses on solving the full coupled equations.

In this paper a new approach is proposed which substantially increases computational efficiency regardless of the numerical solution method used. The key procedure is to uncouple the u

and v equations in such a manner that the uncoupled equations have better convergence properties and also allow more computationally efficient methods to be used in the solution of the implicit equations. Plastic flow can then be obtained by a straightforward time-stepping procedure. This method is based on a semi-implicit treatment of the momentum equations at each level of the modified Euler time step scheme. As shown below, the resulting decoupled implicit equations can be particularly efficiently solved, when, following *Oberhuber* [1990], tridiagonal matrix solvers are used.

This paper gives a description of the method and demonstrates how well it performs in terms of computational efficiency and reasonability of solutions. In addition, the rate of convergence to plastic flow and the dependence of convergence rate upon the maximum creep viscosity parameter are examined. We also note that this method has been extended to a variety of different plastic yield curves [e.g., *Ip*, 1993] other than the elliptical yield curve considered in most of the examples here.

2. Description of the Method

From *Hibler* [1979], sea ice motion is governed by the following momentum balance:

$$m\,\frac{D\mathbf{u}}{Dt} = -mf\mathbf{k} \times \mathbf{u} + \tau_a + \tau_w - mg\nabla_H p(0) + \mathbf{F} \quad (1)$$

where $\mathbf{u} = u\mathbf{i} + v\mathbf{j}$ is ice velocity vector, m is the ice mass per unit area, f is the Coriolis parameter, g is the gravity acceleration, $p(0)$ is the sea surface dynamic height, τ_a is the force due to air stress, τ_w is the nonlinear water drag, $\mathbf{F}$ is the ice interaction force, and $\mathbf{i}, \mathbf{j}$, and $\mathbf{k}$ are the unit vectors in the x, y, and z directions, respectively. The air stress and water stress terms [*McPhee*, 1986] are given by

$$\tau_a = \rho_a C_a |\mathbf{U}_g|(\mathbf{U}_g \cos \phi + \mathbf{k} \times \mathbf{U}_g \sin \phi),$$

$$\tau_w = \rho_w C_w |\mathbf{U}_w - \mathbf{u}|[(\mathbf{U}_w - \mathbf{u}) \cos \theta + \mathbf{k} \times (\mathbf{U}_w - \mathbf{u}) \sin \theta]$$

$$= \tau_w(\mathbf{u}),$$

where $\mathbf{U}_g$ is the geostrophic wind, $\mathbf{U}_w$ is the geostrophic ocean current, C_a and C_w are the air and water drag coefficients, ρ_a and ρ_w are the air and water densities, and ϕ and θ are the air and water turning angles. $\mathbf{F}$ is the force due to internal ice interaction and is given by

$$\mathbf{F} = \nabla \cdot \underset{=}{\sigma}$$

where $\underset{=}{\sigma}$ is the stress tensor (σ_{ij}) which for an isotropic system is related to ice strain rate and strength via a nonlinear viscous-plastic constitutive law:

$$\sigma_{ij} = 2\eta(\dot{\varepsilon}_{ij}, P)\dot{\varepsilon}_{ij} + [\zeta(\dot{\varepsilon}_{ij}, P) - \eta(\dot{\varepsilon}_{ij}, P)]\dot{\varepsilon}_{kk}\delta_{ij} - \frac{P}{2}\,\delta_{ij}$$

In the above equation, $\dot{\varepsilon}_{ij}$ is ice strain rate, given by $\varepsilon_{ij} = 1/2[(\partial u_i/\partial x_j) + (\partial u_j/\partial x_i)]$, P is ice strength which is taken to be a function of ice compactness and thickness, and η and ζ are nonlinear bulk and shear viscosities. These "viscosity" parameters are functions of ice strain rate invariants and ice strength and take on some maximum "creep" value [e.g., *Hibler*, 1979] when the deformation rate becomes very small. The idea here is to approximate rigid behavior by a state of

very slow creep. For the elliptical yield curve used here, the nonlinear viscosities differ from each other by a constant factor, namely $\eta = \zeta/e^2$, where e is a constant and

$$\zeta = 0.5P[(\dot{\varepsilon}_{11}^2 + \dot{\varepsilon}_{22}^2)(1 + e^{-2}) + 4e^{-2}\dot{\varepsilon}_{12}^2$$
$$+ 2\dot{\varepsilon}_{11}\dot{\varepsilon}_{22}(1 - e^{-2})]^{-1/2}$$

In the simulations described in this paper, we have taken $e = 2$ and P to be independent of strain rate. More complex plastic rheologies may be considered by allowing the viscosities to vary in a more complex way and also by allowing P to be a function of deformation invariants [e.g., *Ip et al.*, 1991; *Ip*, 1993; *Song*, 1994]. By appropriate choice of the functional dependence of η, ζ, and P on strain rate, the method can also be adapted to fracture-based yield curves [e.g., *Hibler and Schulson*, 1997].

2.1. Numerical Scheme

For simplicity the numerical method for solving (1) is described in rectangular coordinate system. The method is, however, applicable to the momentum equations in an arbitrary orthogonal curvilinear coordinate system. These curvilinear equations are briefly presented in the next section to demonstrate the structural similarity.

From the constitutive law the ice interaction force components in a cartesian coordinate system are derived as

$$F_x = \frac{\partial}{\partial x}\left\{[\eta + \zeta]\frac{\partial u}{\partial x} + [\zeta - \eta]\frac{\partial v}{\partial y} - \frac{P}{2}\right\}$$
$$+ \frac{\partial}{\partial y}\left[\eta\left(\frac{\partial u}{\partial y} + \frac{\partial v}{\partial x}\right)\right],$$

$$F_y = \frac{\partial}{\partial y}\left\{[\eta + \zeta]\frac{\partial v}{\partial y} + [\zeta - \eta]\frac{\partial u}{\partial x} - \frac{P}{2}\right\}$$
$$+ \frac{\partial}{\partial x}\left[\eta\left(\frac{\partial u}{\partial y} + \frac{\partial v}{\partial x}\right)\right].$$

The component equations of (1) can be organized and simply written as

$$-\frac{\partial}{\partial x}[\eta + \zeta]\frac{\partial u}{\partial x} - \frac{\partial u}{\partial y}\left(\eta\frac{\partial u}{\partial y}\right) + m\frac{\partial u}{\partial t} + C_d u = \tau_x + C_s v$$
$$+ \frac{\partial}{\partial x}[\zeta - \eta]\frac{\partial v}{\partial y} + \frac{\partial}{\partial y}\left(\eta\frac{\partial v}{\partial x}\right) - \frac{\partial P}{\partial x}, \quad (2a)$$

$$-\frac{\partial}{\partial y}[\eta + \zeta]\frac{\partial v}{\partial y} - \frac{\partial}{\partial x}\left(\eta\frac{\partial v}{\partial x}\right) + m\frac{\partial v}{\partial t} + C_d v = \tau_y - C_s u$$
$$+ \frac{\partial}{\partial y}[\zeta - \eta]\frac{\partial u}{\partial x} + \frac{\partial}{\partial x}\left(\eta\frac{\partial u}{\partial y}\right) - \frac{\partial P}{\partial y}, \quad (2b)$$

where C_d and C_s are functions of ice velocity and the viscosities ζ and η are functions of the strain rate invariants. Note that the nonlinear advection terms have been dropped in (2a) and (2b) because they are much smaller than other terms.

At this point it is convenient to describe the various methods for solving these coupled equations. In the original *Hibler* [1979] solutions, (2a) and (2b) were solved simultaneously and implicitly for u and v by point relaxation methods with the C_d, C_s, η, and ζ terms taken to be functions of the ice velocity at the previous time step or, if a modified Euler procedure is used, functions of the ice velocity at the center of the time step. Hence these nonlinear coefficients were taken to be spatially

varying constants in a relaxation solution. A similar procedure is employed by *Oberhuber* [1990] except that more efficient line relaxation methods are used in the implicit solution of the coupled equations. However, while the equations are implicitly solved for all u and v components, since the nonlinear terms have been linearized, a true plastic solution is not obtained unless a number of repetitions of the linearization and relaxation process are made at each time step.

The essential idea presented in this paper is to solve implicitly only the left-hand side of (2a) and (2b) with the terms on the right-hand side taken to be explicitly given by values from the previous time step. This feature effectively decouples the u and v equations and creates a much simpler set of equations to solve implicitly with better convergence properties. While these separate decoupled equations can be solved by point relaxation methods, use of line overrelaxation in conjunction with an implicit tridiagonal matrix solver has been found to be particularly efficient. This decoupling procedure does provide a slightly different solution at each time step than the full semi-implicit method, but since neither method yields directly a plastic solution, it is not a priori clear which solution is better. Also, as we show below, with repetition, both procedures will converge to the same plastic solution. Moreover, in a normal operational time-stepping mode, both methods produce very similar results.

Because more terms are treated explicitly in the splitting method, particular care must be taken in the time-stepping procedure to insure a stable solution for any time step length both for strong and weak ice interaction limits. The approach taken at this point is to first solve the left-hand side of the uncoupled equations (2a) and (2b) implicitly together with the two-level modified Euler time step scheme [*Mesinger and Arakawa*, 1976] which smoothly linearizes and uncouples (2a) and (2b) at each time step. This treatment would, however, leave the combined Coriolis term and off-diagonal water drag term, $C_v \mathbf{u}$, explicit, which is not desirable since it can impose strict limitations on the length of time step interval or result in oscillating solutions in the limit of zero or small ice interaction. To address this issue, a third corrector level solution is adopted which treats the Coriolis term implicitly. As shown in Appendix A, this procedure results in a stable solution independent of time step magnitude.

In order to illustrate the time-stepping procedure, we simplify notation by considering one spatial derivative term in both x and y directions on each side of the u component equation (equation (2a)). The treatment of the v component equation follows a similar manner. Other omitted derivative terms in these equations are treated the same way in time as the ones included. With this abbreviated notation the time-stepping procedure is as follows:

The first level of the modified Euler time step

$$-\frac{\partial}{\partial x}\,\eta(\mathbf{u}^k)\,\frac{\partial u^{k+1/2}}{\partial x} - \frac{\partial}{\partial y}\,\eta(\mathbf{u}^k)\,\frac{\partial u^{k+1/2}}{\partial y} + m\,\frac{u^{k+1/2} - u^k}{\Delta t}$$

$$+ C_d(\mathbf{u}^k)u^{k+1/2} = \tau_x(\mathbf{u}^k) + C_s(\mathbf{u}^k)v^k + \frac{\partial}{\partial x}\,\zeta(\mathbf{u}^k)\,\frac{\partial v^k}{\partial y}. \quad (3)$$

The second level of the modified Euler time step

$$-\frac{\partial}{\partial x}\,\eta(\mathbf{u}^c)\,\frac{\partial u^{k+1^*}}{\partial x} - \frac{\partial}{\partial y}\,\eta(\mathbf{u}^c)\,\frac{\partial u^{k+1}}{\partial y} + m\,\frac{u^{k+1^*} - u^k}{\Delta t}$$

$$+ C_d(\mathbf{u}^c)u^{k+1^*} = \tau_x(\mathbf{u}^c) + C_s(\mathbf{u}^c)v^c + \frac{\partial}{\partial x}\,\zeta(\mathbf{u}^c)\,\frac{\partial v^c}{\partial y}, \quad (4)$$

where $\mathbf{u}^c = (\mathbf{u}^k + \mathbf{u}^{k+1/2})/2$, $u^c = (u^k + u^{k+1/2})/2$, and $v^c = (v^k + v^{k+1/2})/2$.

The third level of correction

$$m\,\frac{u^{k+1} - u^k}{\Delta t} + C_d(\mathbf{u}^c)u^{k+1} - C_s(\mathbf{u}^c)v^{k+1} = \tau_x(\mathbf{u}^c)$$

$$+ \frac{\partial}{\partial x}\,\eta(\mathbf{u}^c)\,\frac{\partial u^{k+1^*}}{\partial x} + \frac{\partial}{\partial y}\,\eta(\mathbf{u}^c)\,\frac{\partial u^{k+1^*}}{\partial y} + \frac{\partial}{\partial x}\,\zeta(\mathbf{u}^c)\,\frac{\partial v^c}{\partial y}. \quad (5)$$

Note that (3), (4), and (5) all are semi-implicit because some of the terms in these equations are calculated using previously obtained ice velocity. However, the solution of (5), which is essential to render Coriolis and off-diagonal water drag terms stable independent of Δt, is quite different from that of (3) and (4). A stability analysis (see Appendix A) shows that application of (5) is sufficient although not always necessary for stable solutions.

In (3) and (4) and the corresponding v component equations not illustrated here, the whole right-hand-side terms are calculated using the previously obtained ice velocity, while the left-hand-side ice velocity components are updated. This treatment effectively uncouples the u and v component equations so that each of the component equations becomes an independent implicit linear equation that can be solved separately. Application of finite difference method to each of them generates a system of simultaneous linear equations of a matrix which is symmetric, positive definite, and of diagonal dominance. This property allows the use of overrelaxation techniques without diverging and hence results in rapid convergence [*Ames*, 1977].

Since (5) is essentially an implicit treatment of the Coriolis term with the ice interaction terms fixed, it can be replaced by the following equation which is easy to solve by algebraic calculations (together with the v component equation):

$$m\,\frac{u^{k+1} - u^{k+1^*}}{\Delta t} + C_d(\mathbf{u}^c)(u^{k+1} - u^{k+1^*}) = C_s(\mathbf{u}^c)(v^{k+1} - v^c). \quad (6)$$

Equation (6) results from (5) minus (4). Note that in the limit of no ice interaction, this procedure reduces to a fully implicit solution of the simple free drift equations. In the case that we wish to keep the inertial terms neutrally damped, the right-hand side may be replaced by

$$\frac{C_s(\mathbf{u}^c)}{2}\,(v^{k+1} - v^c) + \frac{C_s(\mathbf{u}^c)}{2}\,v^c.$$

As shown in Appendix A, this formulation is also numerically stable.

Equations (3) and (4) may be solved by point relaxation or line relaxation together with a tridiagonal solver. If line relaxation is used, a key to the efficient solution of the finite difference equations (3) and (4) is to perform line successive overrelaxation (LSOR) row by row (in x direction) for the u component equations and column by column (in y direction) for the corresponding v component equations. The reason is that the first term in (2a) puts more weight in x direction, while the first term of (2b) has more weight in the y direction. It has been found, for example, that if LSOR is conducted row by row

for the v component equations, the convergence rate can be reduced by a factor of 3 compared to column-by-column relaxation. Taking (3) as an example, it can be rearranged into the following finite difference equation from the spatial finite difference scheme of *Hibler* [1979]:

$$a_{ij}u_{i-1,j}^{k+1/2} + b_{ij}u_{i,j}^{k+1/2} + c_{ij}u_{i+1,j}^{k+1/2} = d_{ij}u_{i,j+1}^{k+1/2} + e_{ij}u_{i,j-1}^{k+1/2} + f_{ij}, \quad (7)$$

where f_{ij} is a summation of the terms that do not depend on $u^{k+1/2}$. Equation (7) can be solved by row-by-row sweeping in conjunction with a tridiagonal solution using, say, the Thomas algorithm for each row. The solution of the v component equations can be obtained in the same way, though with column-by-column sweeping. Essential details of this algorithm for different boundary conditions are given in Appendix B.

For comparison purposes we note that in the original *Hibler* [1979] solution of (2) and (3) by point relaxation, the spatial derivatives and the Coriolis terms were all treated implicitly. This is also true of the *Oberhuber* [1990] method. Also, in the original *Hibler* [1979] paper, calculation of the nonlinear water drag coefficient was not centered in time. However, as noted by *Hibler and Ackley* [1983], with small ice interaction forces the nonlinear water drag term can lead to a spurious splitting solution without the modified Euler centering procedure.

It is also noted that for the special case of no shear viscosity, which occurs for the viscous-plastic solution of the cavitating fluid [e.g., *Flato and Hibler*, 1992], the relaxation sweeping row by row for (3) and (4) and column by column for the v component equations does not require the iterative LSOR procedure but rather one triadiagonal solution to solve the implicit equations. Avoiding iteration, this method becomes extremely computationally efficient for this particular ice rheology.

The three-step solution described above does not necessarily result in plastic solution of ice velocity which is on some occasions desired. In order to obtain plastic solution, "pseudo time steps" can be used with viscosities η and ζ updated at every pseudo time step. By pseudo time step we mean a procedure whereby after one complete modified Euler time step, the final velocity is considered to be the initial velocity in all terms except the inertial term, and the modified time step procedure is then repeated without a change in ice strength. A more efficient pseudo time stepping can also be done by repeating only the second level of the modified Euler time step. At this level the centralized ice velocity, u^c, is still used for calculation of nonlinear water drag. However, the newly obtained velocity (from the first level or the previous pseudo time step) is exclusively used to update η and ζ (and u^c if desired). After a certain number of pseudo time steps, the ice velocity will be close to a plastic solution. The third implicit correction step is still needed, which can be done in the same manner as in (6) with u^{k+1*} being from the last pseudo time step.

2.2. Formulation in Orthogonal Curvilinear Coordinate Systems

This numerical method is also useful for solving the momentum equations in general orthogonal curvilinear coordinate systems. The basic procedure for converting the model to an arbitrary curvilinear coordinate system is to express the ice force and constitutive law in dyadic form valid in any orthogonal curvilinear coordinate system:

$$\mathbf{F} = \underline{\nabla} \cdot \underline{\underline{\sigma}}$$

where

$$\underline{\underline{\sigma}} = \eta(\vec{\nabla}\mathbf{V} + \mathbf{V}\vec{\nabla}) + [(\zeta - \eta)(\nabla \cdot \mathbf{V}) - P/2]\,\underline{\underline{I}} \quad (8)$$

is the stress tensor [*Hibler*, 1979] in dyadic form in terms of the ice velocity $\mathbf{V}$. In a curvilinear coordinate system the gradient operations must include operating on the unit vectors which are also functions of the curvilinear variables [e.g., *Malvern*, 1969]. Here as an example these operations are carried out analytically for a spherical coordinate system. Since this is a two-dimensional (2-D) model, the ice interaction force components in 2-D geostrophic coordinates are derived. By 2-D geostrophic coordinates we mean a spherical coordinate system on the surface of the Earth, without any variation in the radial direction. The results (following *Malvern* [1969] and Appendix B) are given by

$$F_\lambda = \frac{1}{a \cos \varphi} \frac{\partial}{\partial \lambda} \left[(\zeta + \eta)\left(\frac{1}{a \cos \varphi} \frac{\partial u}{\partial \lambda} - \frac{v \tan \phi}{a} \right) \right.$$

$$\left. + (\zeta - \eta)\, \frac{1}{a}\frac{\partial v}{\partial \varphi} - \frac{P}{2} \right]$$

$$+ \frac{1}{a} \frac{\partial}{\partial \varphi} \eta\left(\frac{1}{a}\frac{\partial u}{\partial \varphi} + \frac{u \tan \phi}{a} + \frac{1}{a \cos \varphi}\frac{\partial v}{\partial \lambda} \right)$$

$$- \frac{2\eta \tan \phi}{a}\left(\frac{1}{a}\frac{\partial u}{\partial \varphi} + \frac{u \tan \phi}{a} + \frac{1}{a \cos \varphi}\frac{\partial v}{\partial \lambda} \right), \quad (9a)$$

$$F_\varphi = \frac{1}{a} \frac{\partial}{\partial \varphi} \left[(\zeta + \eta)\left(\frac{1}{a}\frac{\partial v}{\partial \varphi} \right) + (\zeta - \eta) \right.$$

$$\left. \cdot \left(\frac{1}{a \cos \varphi}\frac{\partial u}{\partial \lambda} - \frac{v \tan \phi}{a} \right) - \frac{P}{2} \right]$$

$$+ \frac{1}{a \cos \varphi} \frac{\partial}{\partial \lambda} \eta\left(\frac{1}{a}\frac{\partial u}{\partial \varphi} + \frac{u \tan \phi}{a} + \frac{1}{a \cos \varphi}\frac{\partial v}{\partial \lambda} \right)$$

$$+ \frac{2\eta \tan \phi}{a}\left(\frac{1}{a \cos \varphi}\frac{\partial u}{\partial \lambda} - \frac{v \tan \phi}{a} - \frac{1}{a}\frac{\partial v}{\partial \varphi} \right) \quad (9b)$$

where a is the Earth radius, λ is longitude, and φ is latitude. In (9a) and (9b), η and ζ depend on the invariants of the strain rate tensor $\dot\varepsilon_{ij}$ which in dyadic form is given by $\underline{\dot\varepsilon} = 1/2(\vec\nabla\mathbf{V} + \mathbf{V}\vec\nabla)$. In spherical coordinates the components are given by

$$\dot\varepsilon_{\lambda\lambda} = \frac{1}{a \cos \varphi}\frac{\partial u}{\partial \lambda} - \frac{v \tan \phi}{a}, \qquad \dot\varepsilon_{\varphi\varphi} = \frac{1}{a}\frac{\partial v}{\partial \varphi},$$

$$\dot\varepsilon_{\lambda\varphi} = 0.5\left(\frac{1}{a}\frac{\partial u}{\partial \varphi} + \frac{u \tan \phi}{a} + \frac{1}{a \cos \varphi}\frac{\partial v}{\partial \lambda} \right).$$

Using (9a) and (9b), the momentum equations in spherical coordinates can be derived and decoupled in the same manner as the Cartesian equations (2a) and (2b), and the same three-level time-stepping scheme described earlier may then be used for the solution of the momentum equations. The *Hibler* [1979] spatial finite difference scheme is also usable for (9a) and (9b). Initial tests in spherical coordinates have shown the increase in numerical efficiency due to decoupling to be about the same as in rectangular coordinates.

3. Simulation Results

In order to compare the decoupling method with previous solution methods, a series of ice simulations were carried out on an Alliant FX-80 vector parallel computer. For both for-
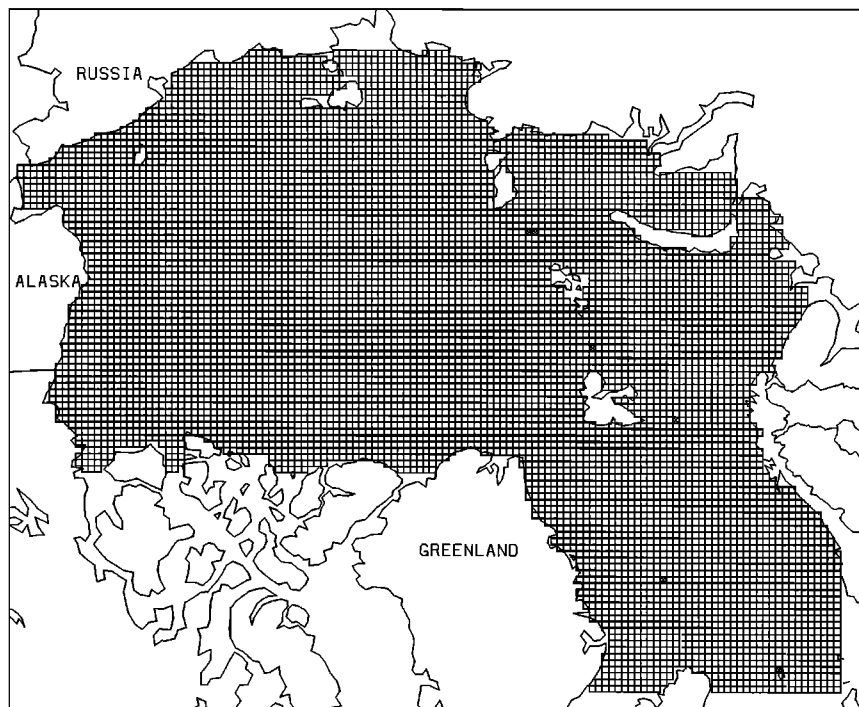
Table 1. Description of the Ice Models

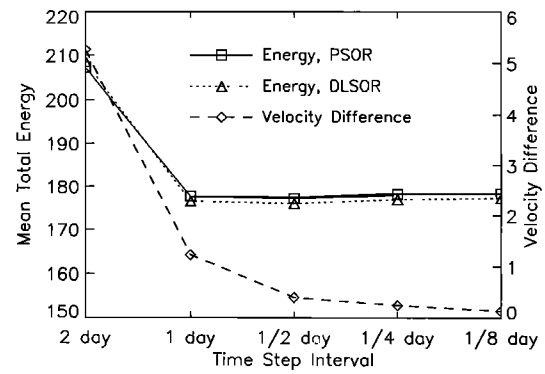|	Resolution	Grid Size	Standard Time Step	Integration
Model 1	80 km	65 × 66	1 day	30 days
Model 2	40 km	130 × 102	1/2 day	10 days

In both models the ice strength is given by $P = P_0 h e^{-C(1-A)}$, where P_0 and C are empirical constants with values of 27.5 k Nm^{-2} and 20. In this equation, h is the mean ice mass per unit area and A is the ice concentration or compactness.

mulations of the equations we examine point relaxation methods. For the decoupled equations we also examine a line successive overrelaxation method combined with a tridiagonal matrix solver. In the decoupled equations these point and line relaxation methods are denoted by DPSOR and DLSOR, while the point relaxation solution for the coupled equations is denoted by PSOR. The Arakawa B grid with velocities at the corner of the grid cells and viscosities at the center was used in all cases [e.g., *Hibler*, 1979]. This grid facilitates coupling with ocean circulation models [e.g., *Hibler and Bryan*, 1987]. The equations may also be formulated in the Arakawa C grid [e.g., *Ip et al.*, 1991].

These three methods are used in two rectangular coordinate ice models with different resolutions that cover the Arctic, Greenland, and Norwegian Seas (see Table 1). Except for resolution, the ice models are similar to the *Hibler* [1979] model and include a coupling to explicit ice concentration and thickness conservation equations. Figure 1 shows the grid configuration of the 40-km resolution ice model. Daily 1981 atmospheric forcing fields are used to drive the ice simulations. More details on the forcing fields are given by *Hibler and Zhang* [1993].
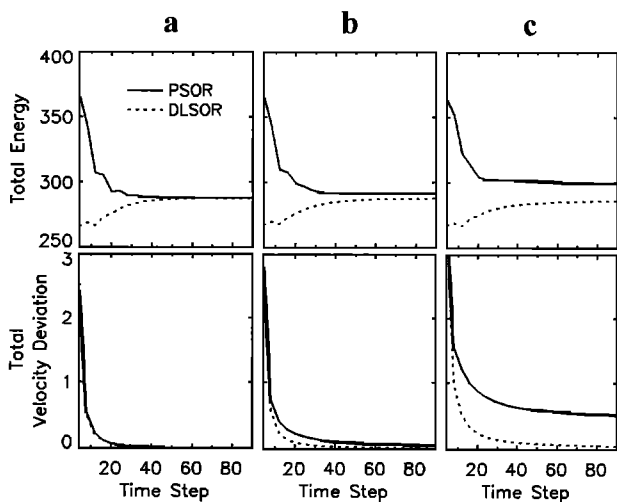

Figure 2. Mean total energy versus time step interval from the ice model of 40-km resolution. The dashed line is for $\Sigma_N \Sigma_M U_{new}^2/N$, the solid line is for $\Sigma_N \Sigma_M U_{std}^2/N$, and the dotted line is for $\Sigma_N \Sigma_M (U_{std} - U_{new})^2/N$ (velocity difference). Here M is the number of total grid points with ice, and N is the number of total time steps.

3.1. Comparisons of Numerical Results

Unless otherwise mentioned we compare the point relaxation solution of the coupled equations (PSOR) with the line relaxation solution of the decoupled equations (DLSOR). However, the other solution method (DPSOR) yields almost identical results for decoupled equations. Since all solution methods involve an overrelaxation parameter, a common value of 1.5 was used in all of these comparisons. The sensitivity of the different methods to the overrelaxation parameter is discussed below.

To examine the overall behavior of the simulated ice velocity field statistically, Figure 2 shows the mean total energy of both methods and mean total velocity difference between both

Figure 1. Grid configuration of 40-km resolution ice model used in the Arctic, Greenland, and Norwegian Seas.

Figure 3. Time series of (top) total energy and (bottom) total velocity deviation from plastic equilibrium using the 40-km resolution model. The total velocity deviation from equilibrium is defined as $\Sigma_M(U - U_e)^2$, where U_e is equilibrium solution at time step 120 from the case in Figure 3a and M is the number of total grid points with sea ice. The solid line is from the PSOR method and the dashed line is from the DLSOR method. The results are from three different convergence criteria or "tolerances": (a) tolerance 2×10^{-6} m s^{-1}; (b) standard tolerance 2×10^{-5} m s^{-1}; (c) 2×10^{-4} m s^{-1}.

methods over 1-month integrations as a function of time step length for the 40-km ice model. The total energy here is defined as a summation of the square of ice velocity at every grid cell with sea ice, and the total velocity difference is defined as a summation of the square of velocity difference between both methods. The concept here is that as the time step becomes smaller, the different semi-implicit treatments converge to the same solution. It is noted from Figure 2 that the total energy values obtained from both methods approach each other and the velocity deviation is diminishing as the time step interval decreases. Half-day time steps for this specific case were good enough to limit the difference to a rather small range.

Since both methods provide an approximation to plastic flow via implicit time stepping, neither result can be considered a priori to be better. As a consequence, perhaps a more critical test of the efficiency of the two methods may be made by comparing the behavior of the two methods when equilibrium plastic ice velocity solutions are approached. For this purpose a sensitivity study was carried out using spatially varying but time invariant winds and ocean currents. In order to examine the plastic equilibrium solution, the ice thickness and compactness were also kept constant. The initial ice velocity (hence the total energy) was set at zero, and the winds were turned on at the first time step.

Shown in Figure 3 are the total velocity deviations from the equilibrium state and the total energy as functions of time. It can be seen from Figure 3 that after the forcing fields are turned on, the total energy from both methods converges to the equilibrium plastic solution rapidly. The more rapid convergence to plastic flow for the DLSOR method has also been verified by Ip [1993] for a variety of other plastic yield curves. Another important feature Figure 3 reveals is that as the tolerance increases, the solutions from the point relaxation method more slowly approach plastic equilibrium. The toler-

ance is the maximum allowable difference between the old and new ice velocity values at the end of an iteration loop. Hence for a lower tolerance the relaxation solution is not a precise solution of the linearized equations. However, if line relaxation is used, then the tridiagonal solution incorporates the boundary conditions into an exact solution of a portion of the difference equations. This likely accounts for reduced sensitivity to tolerance for the line relaxation case.

Finally, we note that the above-mentioned sensitivity study can also be extended to the special case of a cavitating fluid rheology [*Flato and Hibler*, 1992]. With all other parameters kept intact, the shear viscosity was set to be zero so that *Hibler's* [1979] viscous plastic rheology essentially becomes a cavitating fluid, i.e., no shear strength. It should be noted that this formulation of the cavitating fluid differs somewhat from *Flato and Hibler* [1992] in that the bulk viscosity and hence compressive stress depend somewhat on the shear deformation [see *Ip*, 1993]. However, it does serve as a useful comparison of the numerical methods. The performance of both methods in approaching an equilibrium solution is illustrated in Figure 4, where the new method approaches the equilibrium solution faster. The main substantive point here is that with only a bulk viscosity the uncoupling of the equations in the new method allows an exact solution of the separate equations using tridiagonal solution methods without further relaxation.

3.2. Comparisons of Computational Efficiency

Since both methods represent a very similar approximation to plastic flow, what is of main concern is the computational efficiency of the decoupling method. To measure this, we focus on the number of iterations needed for each method. In addition, for direct computer time estimates the CPU time consumed for solving the ice velocity was obtained for each method. Unless otherwise stated, simulations were performed on one computational element of the Alliant FX80 computer so that no concurrentization was employed.

Since all of the solution procedures involve relaxation, a major issue here is the degree to which the solution may be optimized by an appropriate choice of the overrelaxation parameter. To investigate this issue, a series of equilibrium plastic solutions were carried for the 40-km model using different values of the overrelaxation parameter ω. This test involves a 10-day simulation with the initial guess for the solution being at
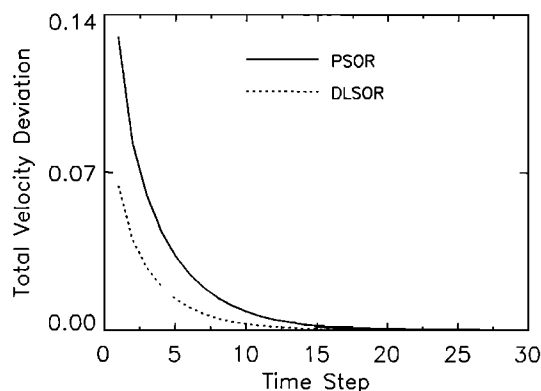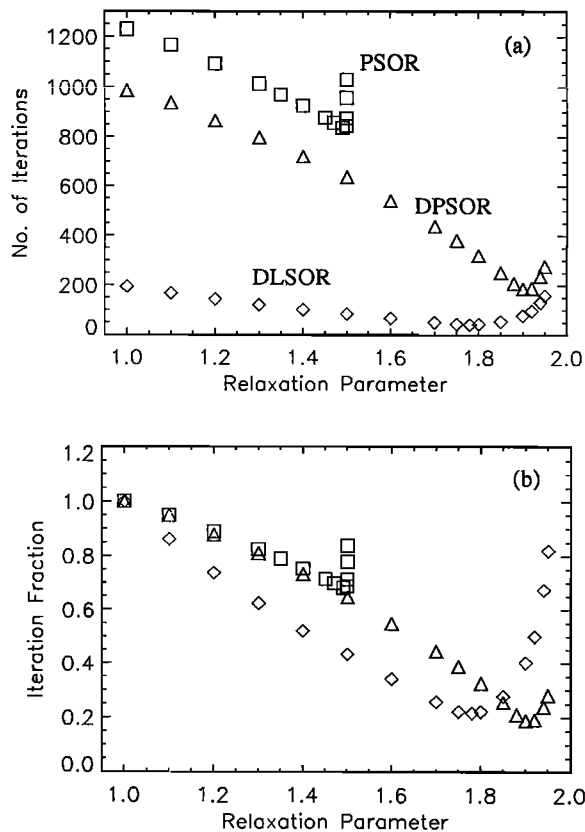

Figure 4. Time series of total velocity deviation from equilibrium using the 80-km resolution model with a "cavitating fluid" rheology. The solid line is from the PSOR method and the dashed line is from the DLSOR method.
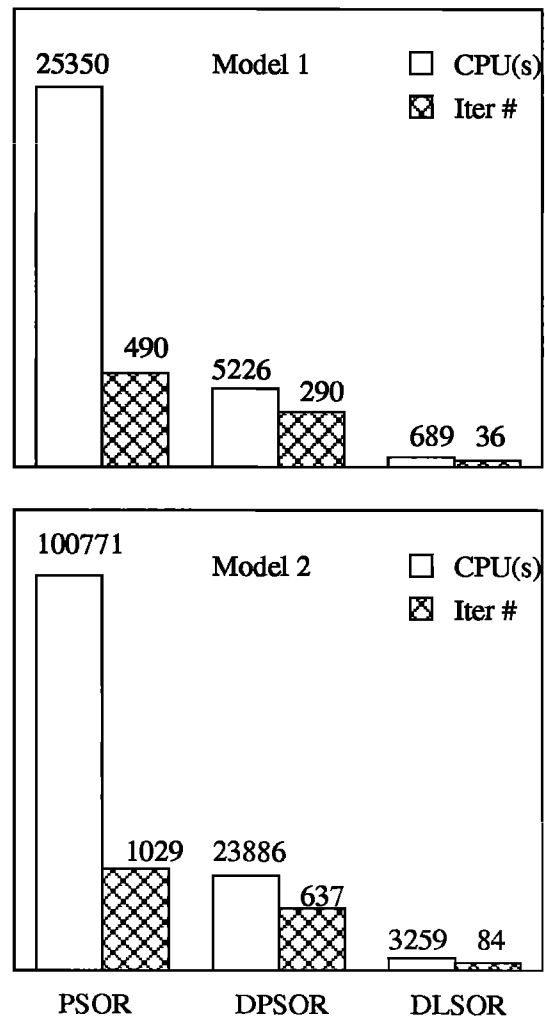
all times a zero velocity field. This is of course a very ineffective way of running an ice model, but it does provide a good comparison of the different convergence rates of the different methods.

The effects of different overrelaxation parameters on computational efficiency are shown in Figure 5a, where we plot the average number of iterations versus the overrelaxation parameter for each method. Because of the superior convergence characteristics of the decoupled equations, it is possible to use a substantially larger overrelaxation parameter than with the coupled equations where the solution is not stable for overrelaxation values greater than 1.5. Comparisons of the relative improvement of each method in Figure 5b show the decoupled line successive overrelaxation technique to have a broad minimum around ω = 1.7. This value of ω yields a solution about 5 times more efficient than the best result for the decoupled point relaxation method which has a sharper minimum around ω = 1.9.

A more practical test of the computational efficiency for the various methods is to use the velocity field at the previous time step for an initial guess. Variations on this method are normally used in time-stepping procedures. To compare this approach with the zero first-guess approach, simulations for the
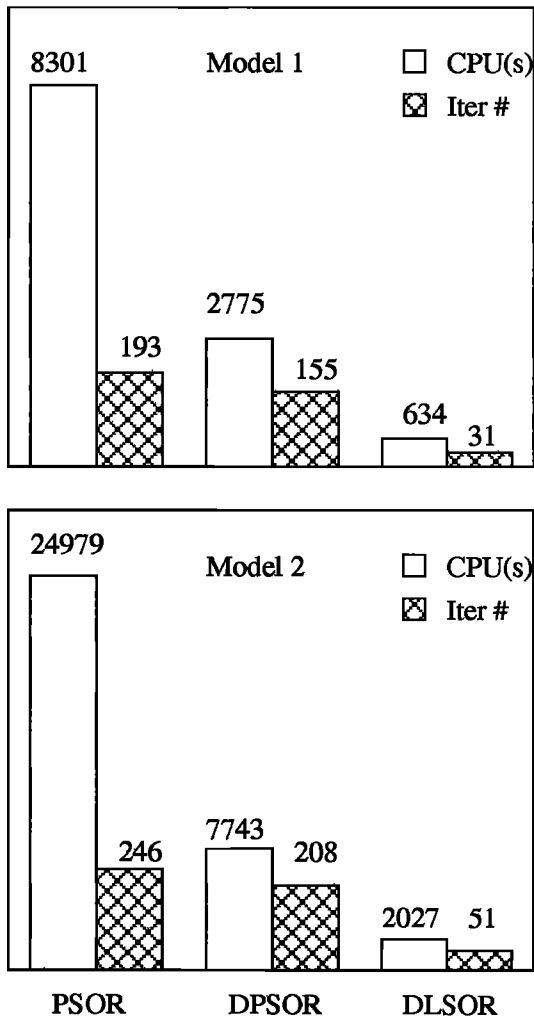

Figure 6. CPU time (in seconds) and average iteration number for each iterative relaxation procedure. The initial guess for the solution before each iterative procedure was a zero velocity field.

Figure 5. (a) Average number of iterations versus overrelaxation parameter for the three numerical procedures and (b) relative fractional improvement for each method compared to straight relaxation. The squares represent the point relaxation method for the coupled equations, while the diamonds and the triangles represent the line and point relaxation methods, respectively, for the decoupled equations. The simulations were performed with the 40-km model over a 10-day interval with a zero first guess for the solution at each time step. The relaxation tolerance was 2 × 10^{-5} m/s.

80- and 40-km resolution models were performed with an overrelaxation parameter of 1.5 for all models. The results are shown in Figures 6 and 7. As can be seen, using a good first guess (Figure 7) yields results relatively similar to the zero first-guess results (Figure 6) except that considerably fewer interations are taken and hence less computer time is used. The decoupling procedure is still considerably more efficient in terms of number of iterations and computer time although now the decoupled point relaxation method is only slightly more efficient than the coupled point relaxation method. However, reference to Figure 5 indicates that this would not be the case if a larger overrelaxation value were used. The decoupled line relaxation is, however, by far the most efficient solution method.

To examine to a limited degree the effects of vectorization and concurrentization on the computational efficiency of the various methods, we compared simulations using different numbers of computational elements on an Alliant FX80 vector parallel computer. The results are shown in Figure 8. In all cases the degree of optimization will represent the degree to which the compiler can vectorize and concurrentize the codes and hence may not represent the maximum efficiency possible.
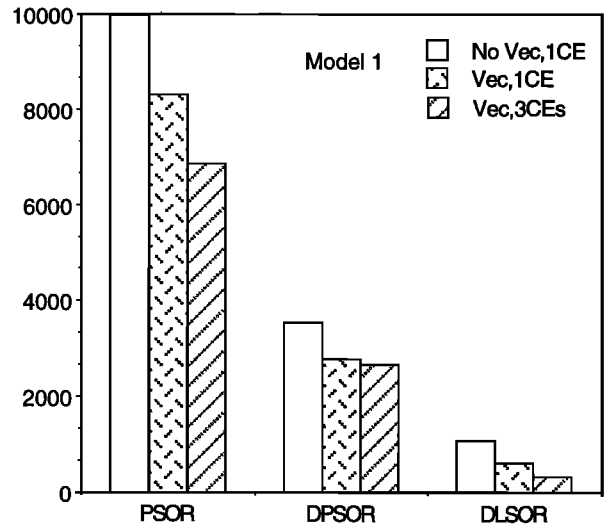
Figure 7. CPU time (in seconds) on one computational element (CE) and average iteration number for each iterative relaxation procedure. The initial guess for solution before each iterative procedure is the velocity field obtained at the previous time step.


Figure 8. CPU time (in seconds) on one CE without vectorization, on one CE with full optimization, and on three CEs with full optimization. The initial guess for solution before each iterative procedure is the velocity field obtained at the previous time step.

Also, other tridiagonal solution techniques may be more optimizable. However, the results do give qualitatively a number of insights.

Basically, vectorization and further concurrentization yield only about a 30% improvement in the speed of the solutions for both point relaxation methods, indicating that most of the computational time is taken up by the nonvectorizable portion of the relaxation procedure. The relative improvement due to vectorization is greater for the DLSOR method, suggesting that there are fewer terms in the relaxation that cannot be vectorized. The DLSOR method also exhibits a speed-up due to parallel processors which is likely due to the u and v equations being simultaneously solved on different computational elements. This efficiency improvement is also in principle possible for DPSOR method with a better optimizing computer. We also note that with the decoupled equations somewhat fewer operations during each relaxation sweep are required than with the coupled equations.

One way to improve the efficiency of the point relaxation methods is to reduce the maximum "creep" viscosity. However, this can create a solution differing substantially from plastic

flow, which is an undesirable effect. This occurs because in the viscous-plastic method [Hibler, 1979] this viscous creep state is used to approximate rigid plastic flow. Numerical experiments were conducted to examine the effect of ζ_{max}, the maximum bulk viscosity, on these two methods in terms of computational efficiency. Basically, the magnitude of ζ_{max} determines how well rigid plastic flow is simulated, with larger values of ζ_{max} providing a better approximation to rigid plastic flow and small values of ζ_{max} representing an ice rheology that is degraded to essentially a linear viscous behavior. The standard value for ζ_{max} in Hibler [1979] is $2.5 \times 10^8 P$, where P is the ice compressive strength. This standard value is large enough to well approximate plastic flow [Hibler, 1979; Ip, 1993] and has been satisfactorily used in arching analysis where the ice is effectively stationary for a long period of time [Ip, 1993].

The effect of ζ_{max} on the two methods is illustrated in Figure 9 where the CPU time in ice dynamics for 1-month integration of the ice-ocean model of resolution 80 km (on one computational element (CE)) is plotted versus the logarithm of $\zeta_{max}/(\zeta_{max})_{standard}$. The PSOR method exhibits a strong dependence on the value of ζ_{max} in the range shown in the plot, whereas the computational effort required by the DLSOR method is weakly dependent on the choice of ζ_{max}. We expect this effect to be due to the line successive relaxation technique. However, the advantage in computational efficiency the DLSOR method has

Table 2. CPU Time for Plastic Solution Using Pseudo Time Stepping for a 1-Month Integration With the DLSOR Method Using Model 1 With a 1-Day Time Step

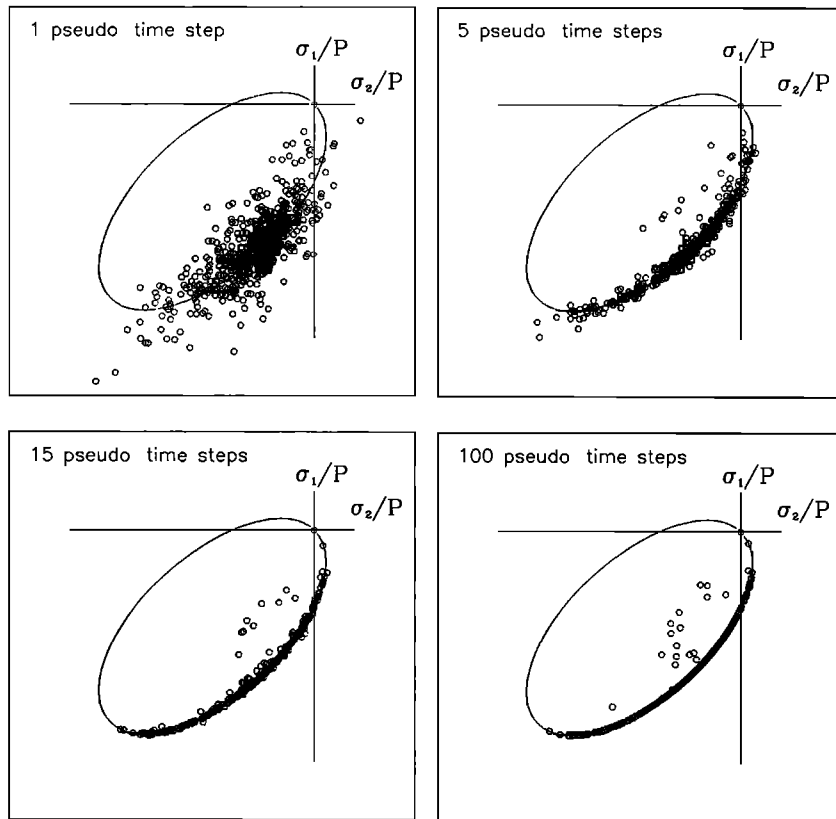| Pseudo Time Step	CPU, s
1	2027
5	4287
10	6018
15	7180
20	8076
30	9449
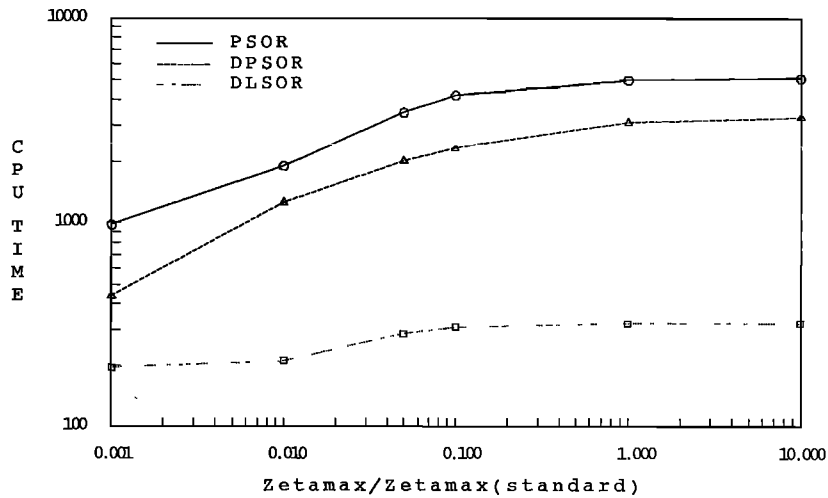
Figure 9. CPU time (in seconds) for the ice dynamics momentum solution for a 1-month integration of the ice model of resolution 80 km (on one CE) versus the logarithm of $\zeta_{max}/(\zeta_{max})_{standard}$ for three different numerical methods.

over the PSOR method is gradually reduced as the ice rheology is degraded into a linear viscous behavior.

3.3. Computational Efficiency of Pseudo Time Stepping

Pseudo time stepping provides an efficient mechanism to obtain fully plastic flow at each time step. The main reasons for this are that it does not require the full modified Euler time

step and that as plastic flow is approached fewer iterations at each pseudo time step are needed. To demonstrate the efficiency of this method, the CPU consumption for plastic solution using pseudo time stepping was examined for model 1 using the decoupled tridiagonal solution procedure. Table 2 shows the consumed CPU time with different numbers of pseudo time steps used. Note that the CPU consumption does

Figure 10. Normalized stress states for different numbers of pseudo time steps using model 2 with 1/4-day physical time steps. The results are from time step 40, and every twelfth spatial point (picked randomly) is plotted.

not increase proportionally with the number of pseudo time steps; this is because that the solution changes slowly at larger pseudo time steps.

In practice, with about 15 pseudo time steps the solutions are quite close to plastic flow. This is illustrated in Figure 10, where we have plotted the normalized stress states for random points from the model 2 computational grid for 1, 5, 15, and 100 pseudo time steps. As can be seen, even five pseudo time steps provide a good approximation to plastic flow for the 1/4-day physical time steps used in this comparison. This result was also verified by examining the total energy versus time. In practice, it is almost impossible to distinguish between energy time series obtained with five and 100 pseudo time steps, respectively.

4. Concluding Remarks

A numerical method for solving viscous-plastic sea ice models has been presented and shown to work substantially more efficiently than previous point relaxation methods. The method is quite general, and while applied here to a particular plastic yield curve, can effectively be used in a wide variety of plastic yield curves as demonstrated by *Ip* [1993]. The method is shown to generate stable solutions in close agreement with joint solution of the coupled equations using point relaxation methods [*Hibler*, 1979]. This is true even if time step interval is not excessively small. Typical solutions from the method demonstrate favorable qualities in terms of rapidly approaching a true plastic equilibrium solution and being relatively insensitive to the accuracy tolerance for a relaxation solution.

The core of the method is the semi-implicit decoupling of the ice momentum equations. This treatment uncouples the u and v sea ice momentum equations so that the remaining implicit equations have better convergence properties and allow more effective iterative methods to be applied. Using a tridiagonal solver in conjunction with a line relaxation technique, the decoupling method is found to converge especially rapidly. Another favorable feature of using tridiagonal solvers is that the CPU consumption does not increase as much as with point relaxation methods as the maximum viscosity increases. The combination of all these features results in a dramatic decrease in computer time and makes viscous-plastic sea ice models more practically usable for finer resolution grids of larger size or for global climatological simulations.

Since this time-stepping procedure involves an updating of the nonlinear viscosities, it also provides a convenient foundation for modeling fully plastic flow by taking a number of pseudo-time steps. In this procedure the forcing fields are kept fixed until the nonlinear viscosities converge to fixed values. In practice, this method allows fully plastic flow to be modeled with only about a threefold to fourfold increase of computer time. Hence this method provides access to a wide variety of plastic ice rheologies other than those considered here.

Appendix A: Stability Analysis

To demonstrate the essential stability characteristics of the time-stepping procedure, it is useful to consider a special case of the momentum equations where the shear and bulk viscosities are spatially constant. For further simplicity, take the water drag coefficients to be constant. With these simplifications the momentum equations become

$$-\zeta \frac{\partial^2 u}{\partial x^2} - \eta \left[\frac{\partial^2 u}{\partial y^2} + \frac{\partial^2 u}{\partial x^2} \right] + m \frac{\partial u}{\partial t} + C_d u = C_s v + \zeta \frac{\partial^2 v}{\partial x \partial y} \tag{A1}$$

$$-\zeta \frac{\partial^2 v}{\partial x^2} - \eta \left[\frac{\partial^2 v}{\partial y^2} + \frac{\partial^2 v}{\partial x^2} \right] + m \frac{\partial v}{\partial t} + C_d v = -C_s u + \zeta \frac{\partial^2 u}{\partial x \partial y} \tag{A2}$$

These equations show that the basic ice interaction coupling between the u and v equations is supplied by the bulk viscosity. Clearly, the essential idea is to move some of the viscous terms to the right of the equation where they are treated explicitly. The issue then is, do we have enough implicit terms left to guarantee stability.

The basic time-stepping procedure consists of a modified Euler time step to deal with the nonlinear terms followed by an implicit corrector step to implicitly solve for the Coriolis and off-diagonal water drag terms. Because of this final implicit time step, in the limit of no ice interaction, the equations would effectively be fully implicit. Since (A1) and (A2) have no nonlinear terms, we only need to consider here a forward time step followed by a corrector step. We proceed by carrying out a Fourier stability analysis where we consider a given Fourier component for u and v and then determine if any amplification factor is greater than one. Since we are interested in the stability for arbitrarily large time steps, we consider $\Delta t \to \infty$ so that the time derivative term may be set equal to zero. Following the Fourier method, consider

$$u = u_o e^{ik_x x} e^{ik_y y}$$

and

$$v = v_o e^{ik_x x} e^{ik_y y}$$

With these assumptions, (A1) and (A2) become

$$(C_d + \zeta k_x^2 + \eta k_y^2 + \eta k_x^2)u + v(\zeta k_x k_y - C_s) = 0 \tag{A3}$$

$$(C_d + \zeta k_y^2 + \eta k_x^2 + \eta k_y^2)v + u(\zeta k_x k_y + C_s) = 0 \tag{A4}$$

The two-step procedure for solving these equations then consists of a provisional step

$$(C_d + \zeta k_x^2 + \eta k_y^2 + \eta k_x^2)u^{(t+1)*} + v^t(\zeta k_x k_y - C_s) = 0 \tag{A5}$$

$$(C_d + \zeta k_y^2 + \eta k_x^2 + \eta k_y^2)v^{(t+1)*} + u^t(\zeta k_x k_y + C_s) = 0 \tag{A6}$$

followed by an implicit corrector step

$$C_d u^{t+1} + (\zeta k_x^2 + \eta k_y^2 + \eta k_x^2)u^{(t+1)*} + v^t \zeta k_x k_y - C_s \theta v^{t+1}$$

$$= C_s \beta v^t \tag{A7}$$

$$C_d v^{t+1} + (\zeta k_x^2 + \eta k_y^2 + \eta k_y^2)v^{(t+1)*} + u^t \zeta k_x k_y + C_s \theta u^{t+1}$$

$$= -C_s \beta u^t \tag{A8}$$

where $\theta + \beta = 1$.

Note that the basic concept in the implicit step is to retain the values of the viscous terms used in the initial time step, while solving implicitly for all the remaining water drag and Coriolis terms.

To show the conditions under which the implicit corrector step for the Coriolis and off-diagonal water drag term is necessary, consider only (A5) and (A6). It is clear that these

equations have an amplification matrix for the (u, v) vector velocity with eigenvalues given by the solution of

$$\lambda^2 = \frac{(\zeta^2 k_x^2 k_y^2 - C_s^2)}{(C_d + \zeta k_x^2 + \eta k_y^2 + \eta k_x^2)(C_d + \zeta k_y^2 + \eta k_x^2 + \eta k_y^2)}$$

If $|C_s| < |C_d|$, the eigenvalues will always have magnitudes less than one, yielding a stable solution. However for $|C_s| > |C_d|$ and k_x and k_y small enough, $|\lambda| > 1$, which is unstable.

For the general stability analysis using (A5) and (A6), the $u^{(i+1)*}$ and $v^{(i+1)*}$ terms may be eliminated from (A7) and (A8). Solving these equations for the (u, v) velocity vector, we obtain

$$u^{i+1} = u^i \frac{C_s(\theta^2 C_s \eta_{yx} + \theta \zeta_{xy} C_d - \theta \beta C_s C_d)}{(C_d + \eta_{yx})(C_d^2 + \theta^2 C_s^2)}$$

$$- v^i \frac{(C_d^2 C_s \beta + C_d^2 \zeta_{xy} - C_d C_s \theta \eta_{xy})}{(C_d + \eta_{xy})(C_d^2 + \theta^2 C_s^2)} \quad (A9)$$

$$v^{i+1} = v^i \frac{C_s(\theta^2 C_s \eta_{xy} - \theta \zeta_{xy} C_d - \theta \beta C_s C_d)}{(C_d + \eta_{xy})(C_d^2 + \theta^2 C_s^2)}$$

$$+ u^i \frac{(C_d^2 C_s \beta - C_d^2 \zeta_{xy} - C_d C_s \theta \eta_{yx})}{(C_d + \eta_{yx})(C_d^2 + \theta^2 C_s^2)} \quad (A10)$$

where $\eta_{xy} = \eta k_x^2 + \eta k_y^2 + \zeta k_y^2$, $\eta_{yx} = \eta k_y^2 + \eta k_x^2 + \zeta k_x^2$, and $\zeta_{xy} = \zeta k_x k_y$.

To simplify the expressions for the eigenvalues of the amplification matrix, consider the case of C_d small which will be the most stringent case. In this case the numerators of the fractions in (A9) and (A10) simplify, yielding

$$u^{i+1} = u^i \frac{C_s(\theta^2 C_s \eta_{yx} - \theta \beta C_s C_d)}{(C_d + \eta_{yx})(C_d^2 + \theta^2 C_s^2)} \quad (A11)$$

$$v^{i+1} = v^i \frac{C_s(\theta^2 C_s \eta_{xy} - \theta \beta C_s C_d)}{(C_d + \eta_{xy})(C_d^2 + \theta^2 C_s^2)} \quad (A12)$$

In (A11) and (A12) we have retained the C_d terms in the numerator only where they are necessary to keep the numerator finite in the limit of k_x, $k_y \rightarrow 0$. Clearly, the amplification factors for u and v are less than one for $\theta \geq 1/2$. In the limit of k_x, $k_y \rightarrow 0$, however, the amplification factors will be less than one for $\theta < 1/2$ and C_d small enough.

The small C_d limit can be verified by an exact solution of the eigenvalues of the amplification matrix in (A9) and (A10). By setting the magnitudes of the eigenvalues equal to one and examining the equation, we find that λ can have magnitude 1 or larger only if

$$\frac{C_d}{C_s} \leq \sqrt{1 - 2\theta}$$

where $\theta \leq 1/2$ and the equality holds in the limit of k_x, $k_y \rightarrow 0$, which is the most unstable case.

Appendix B: Line Relaxation Using the Thomas Algorithm

Referring back to (7), for a given row we wish to solve the following equation for the x velocity component u:

$$a_i u_{i-1} + b_i u_i + c_i u_{i+1} = d_i \quad (B1)$$

where u_i is the x velocity in the ith column and d_i depends on either u velocities in other rows or on v velocity components. Given Dirichlet boundary conditions, we wish to solve this set of linear equations for $i = 2$ to $n - 1$ subject to boundary conditions of specified u_1 and u_n. Without loss of generality we may consider the case of $u_n = u_1 = 0$ by the appropriate redefinition of d_i. In this case, a_i, b_i, c_i, and d_i are defined for $i = 2$ to $n - 1$. To solve this set of equations, we make use of a particular application of the Thomas Algorithm, an iterative Gaussian elimination procedure which requires two iterative sweeps through the row: once in a forward direction and then once in a backward direction. For the forward sweep we solve for two indexed constants g_i and f_i by first taking

$$g_2 = c_2$$

$$f_2 = d_2/b_2$$

and then for $i = 3$ to $i = n - 1$:

$$g_i = \frac{c_i}{(b_i - a_i)g_{i-1}}$$

$$f_i = \frac{d_i - a_i f_{i-1}}{b_i - a_i g_{i-1}}$$

The solutions of u_i for these boundary conditions are then obtained by a backward sweep:

$$u_{n-1} = f_{n-1} \quad (B2)$$

and for $i = 2$ to $n - 2$

$$u_{n-i} = f_{n-i} - g_{n-i} u_{n-i+1} \quad (B3)$$

For row overrelaxation, denoting by u_i' the values of u_i before the Thomas Algorithm was applied to this row, we replace u_i' in this row by u_i'', where

$$u_i'' = u_i' + w(u_i - u_i') \quad (B4)$$

and w is an overrelaxation parameter (~ 1.8 for maximum efficiency) and the values of u_i are obtained from (B2) and (B3). The next row is then solved for in the same way as in (B1) thru (B4). A similar procedure can be used for the y velocity component equations except that column relaxation is used. In the case of $w = 1$, block relaxation may also be used in (B4).

The standard boundary condition is to specify a zero velocity Dirichlet boundary condition at land boundaries which with the nonlinear plasticity will naturally allow an effective discontinuous slip to occur there [*Hibler*, 1979]. Open free ice edge boundaries can naturally be handled dynamically by simply setting the ice strength equal to zero next to an artificial land boundary. A free slip boundary may be effected by using the cavitating fluid formulation discussed in the text at grid cells next to a land boundary.

References

Ames, W. F., *Numerical Methods for Partial Differential Equations*, Academic, San Diego, Calif., 1977.

Coon, M. D., S. A. Maykut, R. S. Pritchard, D. D. Rothrock, and A. S. Thorndike, Modeling the pack ice as an elastic-plastic material, *AIDJEX Bull.*, *24*, 1–105, 1974.

Flato, G. M., and W. D. Hibler III, Modeling pack ice as a cavitating fluid, *J. Phys. Oceanogr.*, *22*, 626–651, 1992.

Hibler, W. D., III, A dynamic thermodynamic sea ice model, *J. Phys. Oceanogr.*, *9*, 815–846, 1979.

Hibler, W. D., III, and S. F. Ackley, Numerical simulation of the Weddell Sea pack ice, *J. Geophys. Res.*, *88*, 2873–2887, 1983.

Hibler, W. D., III, and K. Bryan, A diagnostic ice-ocean model, *J. Phys. Oceanogr.*, *17*, 987–1015, 1987.

Hibler, W. D., III, and E. M. Schulson, On modeling sea ice fracture and flow in numerical investigations of climate, *Ann. Glaciol.*, in press, 1997.

Hibler, W. D., III, and J. Zhang, Interannual and climate characteristics of an ice-ocean circulation model, in *Ice in the Climate System*, *NATO ASI Ser. I*, vol. 112, edited by W. R. Peltier, pp. 633–651, Springer-Verlag, New York, 1993.

Holland, D. M., L. A. Mysak, K. Manak, and J. M. Oberhuber, Sensitivity study of a dynamic thermodynamic sea ice model, *J. Geophys. Res.*, *98*, 2561–2586, 1993.

Ip, C. F., Numerical investigation of different rheologies on sea-ice dynamics, Ph.D thesis, Dartmouth Coll., Hanover, N. H., 1993.

Ip, C. F., W. D. Hibler III, and G. M. Flato, On the effect of rheology on seasonal sea ice simulations, *Ann. Glaciol.*, *15*, 17–25, 1991.

Malvern, L. E., *Introduction to the Mechanics of a Continuous Medium*, 713 pp., Prentice-Hall, Englewood Cliffs, N. J., 1969.

McPhee, M. G., The upper ocean, in *The Geophysics of Sea Ice*, edited by N. Untersteiner, pp. 339–394, Plenum, New York, 1986.

Mesinger, F., and A. Arakawa, Numerical methods used in atmospheric models, vol. I, 13 pp., *GARP Publ. Ser. 17*, World Meteorol. Organ./Int. Counc. of Sci. Unions Joint Organizing Comm., Geneva, Switzerland, 1976.

Oberhuber, J. M., Simulation of the Atlantic circulation with a coupled sea ice-mixed layer-isopycnal general circulation model, *Rep. 59*, Max-Planck-Inst. for Meteorol., Hamburg, Germany, 1990.

Pritchard, R. S., M. D. Coon, and M. G. McPhee, Simulation of sea ice dynamics during AIDJEX, *J. Pressure Vessel Technol.*, *99J*, 491–497, 1977.

Song, X., Numerical investigation of a viscous plastic sea-ice forecasting model, M.S. thesis, Dartmouth Coll., Hanover, N. H., 1994.

Thorndike, A. S., and R. Colony, Sea ice motion in response to geostrophic winds, *J. Geophys. Res.*, *87*, 5845–5852, 1982.

W. D. Hibler III, Thayer School of Engineering, Dartmouth College, 8000 Cummings Hall, Hanover, NH 03755-8000. (e-mail: whibler@dartmouth.edu)

J. Zhang, Polar Science Center, University of Washington, Seattle, WA 98105. (e-mail: zhang@apl.washington.edu)